

# Plasmonic logic gates and devices in silver nanowire networks

Hong Wei, Hongxing Xu\*

Beijing National Laboratory for Condensed Matter Physics and Institute of Physics, Chinese Academy of Sciences, Box 603-146, Beijing 100190, China

## ABSTRACT

The local electric field distribution of propagating surface plasmons along Ag nanowires can be imaged by coating the nanowires with a layer of quantum dots, which provide a useful tool to study the plasmon propagation. In simple photonic networks composed of Ag nanowires, plasmons can be controllably routed to a specific nanowire output. The underlying physical mechanism is that the plasmon interferences modulate the near field distribution and thus control the output intensity. The plasmon interference can result in combinations of optical signals that execute specific interferometric Boolean logic operations. And a complete family of Boolean logic gates is realized in the simple nanowire networks. The primary nanowire in the network can be viewed as the plasmonic equivalent of a bus in a central processing unit. Furthermore, a plasmonic NOR gate is demonstrated by cascading OR gate and NOT gate. To realize the cascaded NOR gate, the plasmon wave packet should overlap with the junction between the main wire and the branch wire for the control signal.

**Keywords:** plasmons, logic gates, nanowire, network, interference, cascade, quantum dots

## 1. INTRODUCTION

Nobel metal nanostructures have many unique properties due to surface plasmon resonances, and have been used in different fields, such as surface-enhanced spectroscopy [1-4], plasmon-assisted optical force [5-7], biological sensing [8-10], cancer therapy [11] and photovoltaic devices [12]. We have focused on the mechanism of strong electromagnetic near field enhancement by surface plasmon resonances and its applications for more than one decade. The excitation of surface plasmons in metal nanostructures can generate enhanced electromagnetic field [13], especially when the metal nanoparticles are placed nearby [14-18]. For a nanoparticle dimer, the electromagnetic coupling between the two particles will make the electromagnetic field in the dimer junction be enhanced greatly. This large field enhancement makes single molecule surface-enhancement Raman scattering (SERS) possible [14, 15]. Besides single nanoparticles and nanoparticle dimers [19-21], nanostructures of other different geometries have been investigated, such as core-shell nanoparticles [22-25], nanoparticle arrays [26, 27], nanohole-particle [28], nanowire-nanoparticle [29], nanotip-nanoparticle [30, 31], nanoparticle chain [32, 33], nanoparticles deposited on nanowire arrays [34]. Particles with rough surface are also good structures for SERS [35, 36]. It has been reported that the nanoparticle aggregates can serve as antennas to modulate the emission polarization of single molecule [37, 38]. The SP resonances strongly depend on the nanostructure size, shape, morphology and dielectric environment [39-42]. The SP resonance peak shift with change of the dielectric environment caused by adsorption of molecules or different dielectric coating thickness makes it a useful tool for sensing [8, 9].

Recently, one dimensional metal nanowires (NWs) are attractive because they support propagating SPs [43-47]. For nanowires with diameter smaller than half wavelength of the input light, they can realize the light propagation with the local field tightly confined around the nanowires. And the light emission from a nanowire occurs only at the ends of the structure and other symmetry-breaking sites, such as an adjacent nanoparticle, a structural anomaly [44, 45]. We recently

\*hxxu@iphy.ac.cn

demonstrated that by using propagating SPs on metal nanowires, SERS and quantum dot fluorescence can be remotely excited [48, 49]. The propagating SP emission direction, correlation between incident and emission polarization, emission modulation, effect of a proximal substrate and coloring fluorescence emission have also been investigated [50-55]. In branched NW structures composed of a primary NW and a branch NW, the plasmons can be routed to either output terminal by controlling the incident polarization [56]. On the other hand, the coupling of light to SPs makes it possible to reduce the dimensions of light-based devices to the nanoscale. Plasmonic waveguide provides an important element to build plasmonic circuits [57, 58].

In this paper, we will discuss the plasmonic logic operations realized in Ag NW networks and the underlying mechanism. By using QD fluorescence, the local electric field distribution of propagating SPs along Ag NWs can be imaged [57]. This provides a valuable tool for the study of plasmons propagating along branched or joined NWs, forming NW networks. In Ag NW networks of simple geometries, plasmons launched at two input terminals can be controllably routed to a specific NW output [57]. The underlying physical mechanism, interference between SPs launched at different positions along a primary NW, is clearly observable, as is the detailed evolution of the plasmon field along the device. If a second plasmon beam is excited in the simple NW network, the output can be controlled to turn on or turn off, which results in combinations of optical signals that execute specific interferometric Boolean logic operations. This primary NW can thus be viewed as the plasmonic equivalent of a bus in a central processing unit. By loading the primary NW with plasmons launched with specific input properties at the secondary input NWs, the resulting plasmonic interference enables routing and out-coupling to specific output NWs. Furthermore, we demonstrated that the plasmonic logic operations can be cascaded. A NOR gate is realized by cascading OR and NOT gates in a four terminal NW network [58]. QD imaging reveals that the control to plasmon near-field distributions play an important role in determining the performance of the device.

## 2. QUANTUM-DOT BASED LOCAL FIELD IMAGING FOR PLASMONS ON SILVER NANOWIRES

Chemically synthesized Ag nanowires (NWs) with smooth surfaces are excellent waveguides that support propagating SPs. The Ag NWs are dispersed on clean glass substrate, and  $\text{Al}_2\text{O}_3$  was deposited onto the sample using atomic layer deposition (ALD) technique. Then, CdSe@ZnS quantum dots (QDs) are spincoated on top of the sample as local reporters to image the electromagnetic (EM) near-field distribution on the NWs.

A bright field image of a typical Ag nanowire and its QD emission image under large-area illumination are shown in Figure 1ai, ii. When a 632.8 nm laser is focused at one end of the nanowire, a periodic node-like field distribution along the wire is clearly observed (Figure 1aiii-vi). The spatial modulation of the near field along the nanowire is a direct result of the interference of the wire plasmons excited by the light source. The excitation light with arbitrary polarization can excite plasmons of different modes, the spatial distribution of which is quite different. The interference of these modes results in the modulated electric field distribution along the NW. The excitation efficiency and thus the magnitude of a certain mode can be determined by incident polarization. Therefore the total local field distribution is strongly dependent on the polarization direction of the laser input. For longitudinal incident polarization (Figure 1aiii), the near field is distributed symmetrically along the NW. Increasing the polarization angle shifts the well-pronounced nodes of the field distribution from one side of the NW to the other.

If a structural anomaly, such as an adjacent Ag nanoparticle, is present near a node of the NW plasmon, it can affect the plasmon field distribution, and result in bright emission, as shown in Figure 1b. The strength of the far-field emission at the adjacent nanoparticle is strongly controlled by the local plasmon-induced field distribution. Here, changing the polarization angle of the plasmon-launching laser controls the light emission intensity from the adjacent Ag nanoparticle. Light emission from the nanoparticle can be varied from a maximally emitting "ON" state (Figure 1biii), when the node of the field distribution is at the particle (Figure 1biv), to a minimally-emitting "OFF" state (Figure 1bv), when the node is on the opposite side of the nanowire (Figure 1bvi).

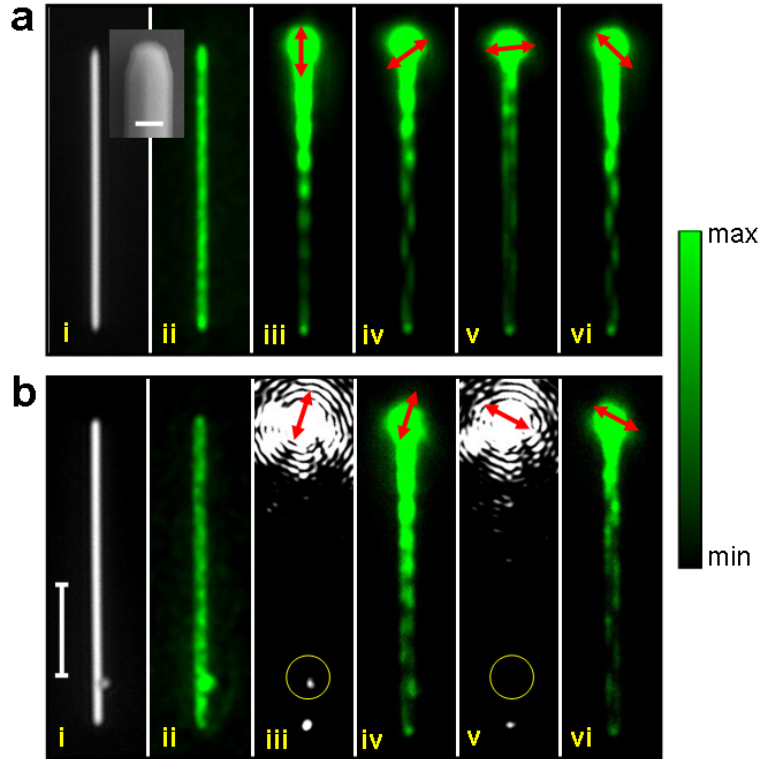


Figure 1. QD emission images of plasmons launched by 632.8 nm laser excitation at one end of a Ag nanowire. Changing the polarization angle at the input modifies the field distribution in the nanowire (a) and controls the emission from an adjacent Ag nanoparticle at the opposite end of the wire (b). (a) (i) Optical image of a NW and a SEM image of a typical NW coated with 30 nm Al<sub>2</sub>O<sub>3</sub> (inset). (ii) The QD emission image with wide field excitation. (iii-vi) QD emission images for different incident polarizations. (b) (i) Optical image of a NW-NP system. (ii) The QD emission image with wide field excitation. (iii) Scattering image. (iv) QD emission image corresponding to (iii). (v,vi) Scattering and QD emission images for a different polarization. The scale bar is 200 nm in ai, and 5  $\mu$ m in bi. The red arrows indicate the laser polarization. To enhance the contrast, we use a green color scale to show the intensity distribution of the QD emission. (ref 57)

### 3. INTERFEROMETRIC LOGIC IN SILVER NANOWIRE NETWORKS

When a second nanowire is placed in close proximity to the primary wire in a branching geometry, it can serve as a second input from which a plasmon can be independently launched onto the structure (Figure 2a). We can describe the behavior of this simple branched nanowire as having two input terminals I1 and I2 and one output terminal (O). Both the polarization angle and the phase difference between the two excitation beams I1 and I2 control the emission at output O. As the relative phase between I1 and I2 is monotonically increased, the emission intensity at O varies in an oscillatory manner (Figure 2b). For the specific input polarizations shown in Figure 2, the ratio of maximum to minimum intensity at O can be larger than 10. This dynamic range makes it straightforward to assign maximum and minimum output intensities as “ON” and “OFF” states. When the two input fields (1 and 1) individually or collectively result in a maximum (1), this three-terminal structure represents an OR gate. Conversely, either input signal will emit when launched individually but, when launched jointly, may result in a minimum or “OFF” state (0) when the two input plasmons interfere destructively. In this case, the structure functions as an XOR gate. The QD emission images for these “ON” and “OFF” states (Figure 2c) clearly show the underlying interference-based mechanism resulting in the observed output behavior.

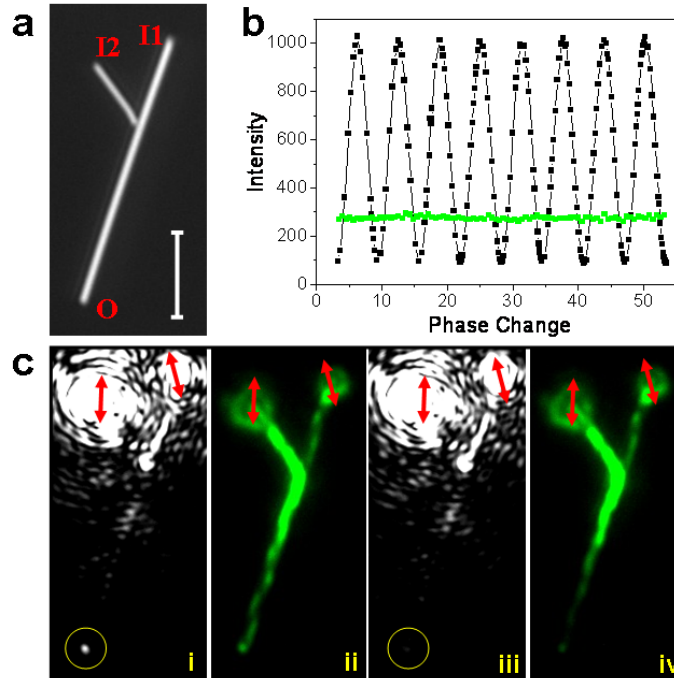


Figure 2. Interference of plasmons in Ag NWs. (a) Optical image of a simple two-nanowire network composed of a primary nanowire and a converging secondary input nanowire. (b) Scattering intensity at output O as a function of optical phase delay when input is either I1 or I2 (green); scattering intensity at output O as a function of optical phase delay for both I1 and I2 inputs (black). (c) (i,iii) Scattering images for the case of two inputs I1 and I2, but with differing phase change. (ii,iv) QD emission images corresponding to i and iii. The red arrows indicate the polarization of the input excitation laser. The  $\text{Al}_2\text{O}_3$  thickness is 30 nm, and the scale bar is 5  $\mu\text{m}$ . (ref 57)

A more complex plasmonic device consisting of a primary wire with two additional branches, one input and one output, is shown in Figure 3a. For this structure, the wire ends marked with I1 and I2 function as inputs while the positions labeled O1 and O2 serve as outputs. For the two incident light polarizations indicated by the red arrows, maximum light emission is varied from O1 and O2 as a function of the relative phase of the two input fields (Figure 3b). This behaviour can be understood directly from the QD emission images in Figure 3c. The output from O2 is controlled by the intensity of the field in the wire junction (encircled by the dashed yellow rectangle), and the output from O1 is determined by the field intensity at the end of the primary wire. The O1 and O2 emission intensities over several cycles of relative phase (2  $\pi$ /cycle) of the two inputs are shown in Figure 3d. By defining specific intensity thresholds for “ON” and “OFF” states for the structure in Figure 3, additional logic gates can be realized. For example, for an intensity threshold of 450 a.u., and considering O2 as the output, (I1=“ON”, I2=“OFF”) results in O2=“OFF”, (I1=“OFF”, I2=“ON”) results in O2=“OFF”, and (I1=“ON”, I2=“ON”) input results in O2=“ON”, demonstrating the behavior of an AND gate.

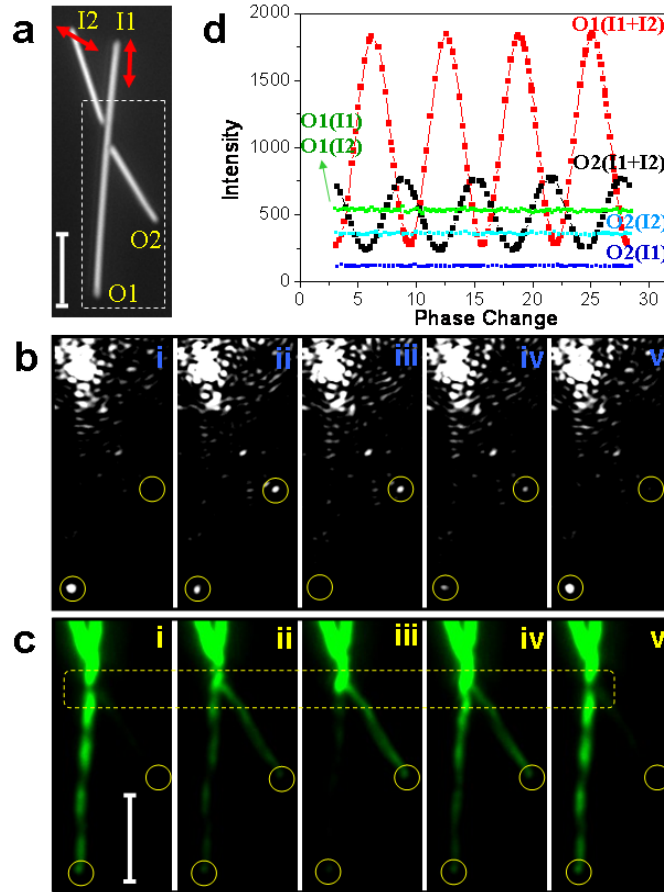


Figure 3. Modulation and routing of light in a two input-two output nanowire network. (a) Optical image of the network. (b) Scattering images for two beam interference in one cycle. (c) QD emission images in one interference cycle. (d) Scattering intensity at O1 and O2 terminals. Red, the intensity of O1 for simultaneous input of both I1 and I2; black, the intensity of O2 for simultaneous input of I1 and I2; green, the intensity of O1 for I1 only and I2 only; cyan, the intensity of O2 for I2 only; blue, the intensity of O2 for I1 only.  $\text{Al}_2\text{O}_3$  thickness is 50nm, scalebar is  $5\mu\text{m}$ . Red arrows in (a) show the polarization of the two laser beams, and the white dashed rectangle in (a) mark the area displayed in (b, c). (ref 57)

A summary of a few of the many logic functions that can be demonstrated in branched nanowire structures is provided in Table 1. The logic gates AND, OR, and NOT, shown here, are sufficient to realize all binary logic functions. As shown earlier, OR and XOR gates are related to each other, differing at one input by half a plasmon wavelength. Here we also illustrate how the system in Figure 3 can be regarded as a binary adder, where two inputs (1+1) result in outputs of 1 (the intensity threshold is defined as  $> 500$ ) at output O2 and 0 at output O1:  $1+1=10$ . Only one above-threshold signal at either input results in 1 at O1 and 0 at O2:  $0+1=1+0=01$ .

Table 1. Examples of All-Optical Logic Operations Based on NW Networks<sup>a</sup> (ref 57)

AND				
OR				
XOR				
NOT				
NAND				
Adder				
	$0+0=(0\ 0)$	$0+1=(0\ 1)$	$1+0=(0\ 1)$	$1+1=(1\ 0)$

<sup>a</sup> The numbers in red are inputs and the numbers in blue are outputs. Unused terminals are labeled empty. The terminals labeled control require the input to be ON.

#### 4. CASCADE OF PLASMONIC LOGIC GATES

The logic operations have been realized by utilizing polarization and phase-dependent interference between plasmon beams propagating through the wire network. But more complex logic functions and functional photonic circuits rely on the possibility of cascading the basic gates. A particularly important step in this direction is the construction of so-called universal gates, that is NAND and NOR gates, which can be combined to implement essentially any logic operation. Figure 4a illustrates the schematics of cascaded plasmonic OR and NOT gates for the universal logic gate NOR. It has been demonstrated that the interferences of two plasmon beams in single branched Ag NW structure can function as OR or NOT gates. Here, we arranged Ag NWs with a micromanipulator to construct a four terminal NW structure composed of a primary NW and two branch NWs as shown in Figure 4b. The first branch NW with the terminal marked as “I2” and the first half part of the primary NW with terminal marked as “I1” form the first branched structure, which is designed to function as an OR gate. The second branch NW with the terminal marked as “C” and the last half part of the primary NW forms the second branched structure, which is designed to be a NOT gate. The experimental setup was schematically shown in Figure 4c.

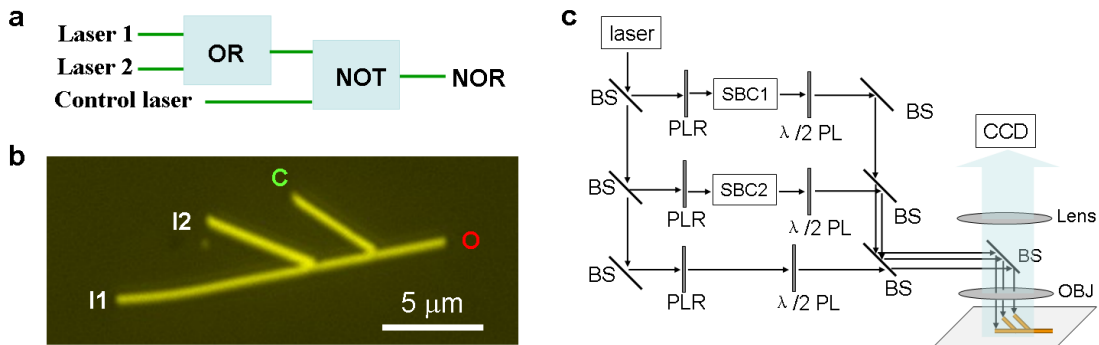


Figure 4. Cascaded logic gates for NOR gate and the experimental setup. (a) Schematic illustration of logic gate NOR built by cascaded OR and NOT gates. (b) Optical image of the designed Ag NW structure. (c) Schematics of experimental setup.

Figure 5a shows the output intensity for different inputs. For a particular given phase of I1 and I2, the outputs  $O(C, I1)$ ,  $O(C, I2)$ , and  $O(C, I1, I2)$  are simultaneously minimized (red lines in Figure 5ai, ii and iii), while the output  $O(I1, I2)$  is close to maximum (green line in Figure 5aiv). If we define a scattering intensity from the output terminal of  $> 200$  as the “1” or “ON” state, e.g. the value above the green dot lines ( $O(I1)$ ,  $O(I2)$ ,  $O(C)$ ) in Figure 5a, and the intensity  $< 200$ , e.g. the red lines as “0” or “OFF” state, then all of the two inputs interference and the three inputs interference result in “0” output for certain input phases. To illustrate the optical binary logic NOR gate, we treat terminal I1 and I2 as the input ends for the signals, and terminal C as the control end. For any input from either I1 or I2 only, the control C will invert it, i.e. invert “0” to “1”, or “1” to “0”. Hence, if we have input variables from (I1, I2): (0, 0), (1, 0), (0, 1), (1, 1), the output is 1, 0, 0, 0, respectively. That is the Boolean logic gate NOR. The scattering images for different inputs are shown in Figure 5b-d, which clearly show that the NOR gate is cascaded by the OR gate and NOT gate.

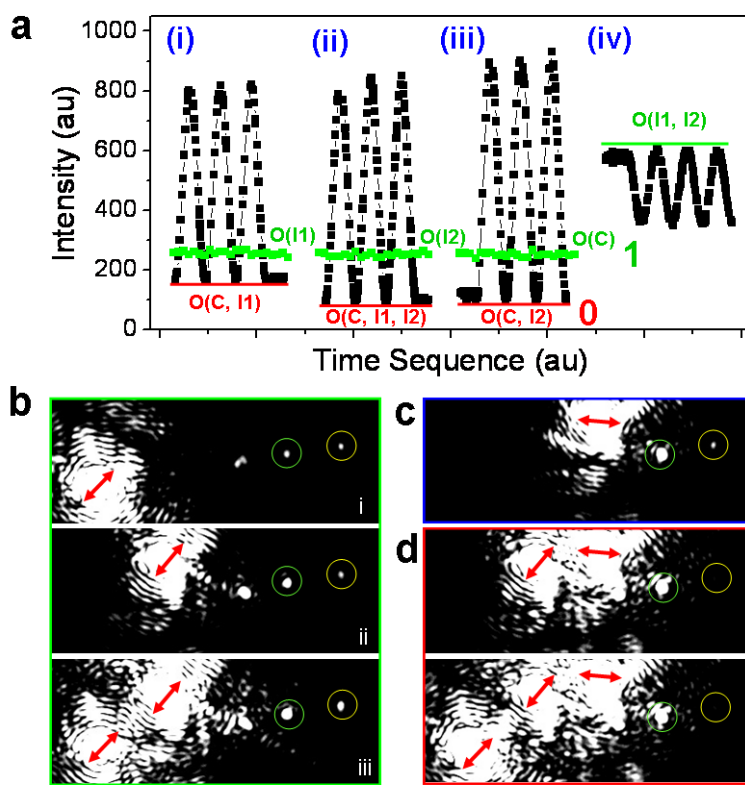


Figure 5. Output intensity at the O end for different inputs versus the time sequence as the incident phases are changed. (a) The output intensity for the inputs from terminals (C, I1), (C, I1, I2), (C, I2) and (I1, I2). The red lines emphasize the output intensity for the NOR operation. The green line emphasizes the corresponding output intensity for (I1, I2). (b) The scattering images showing the OR operations. (c) The scattering image when only C was enabled. (d) The scattering images for the NOR operations, corresponding to a NOT function acting on bii and biii. The red arrows show the incident laser polarization. The green and yellow circles mark the C branch junction and the O terminal, respectively. (ref 58)

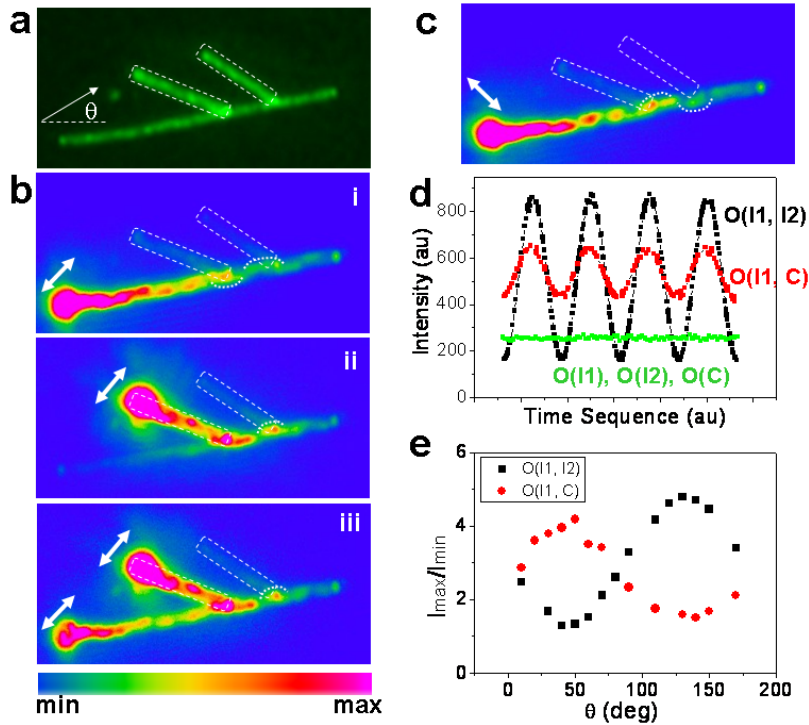


Figure 6 Dependence of plasmon interference on incident polarizations. (a) QD fluorescence image by wide field illumination. Dashed white lines show the outline of the branch NWs. (b, c) QD fluorescence images with excitation at different terminals with polarization indicated by the white arrows. (d) The output intensity at terminal O as a function of the phase difference between two laser beams. Green: the output intensity when only one input (I1, I2, or C) is applied. Black: the output intensity resulting from two incident beams (I1 and I2). Red: the output intensity resulting from two incident beams (I1 and C). The incident polarizations at I1 and I2 terminals used for this set of measurement corresponds to the polarizations shown in c and bii. The incident polarization at C terminal is the same as in Figure 5. (e) Interference depth of (I1, I2) and (I1, C) as a function of polarization angle  $\theta$  of the input laser at the I1 terminal. The definition of  $\theta$  is shown in (a). The polarizations of I2 and C are kept the same as those in Figure 5. (ref 58)

In order to understand the mechanism of cascaded plasmonic logic devices, we use QD fluorescence to image the EM near-field distribution of the propagating plasmons on metal NWs. Figure 6a shows the QD fluorescence image by a wide field excitation, which indicates an even distribution of QD coating on the NWs. The white dashed lines show the outline of the branch NWs. The white dotted curved lines in Figure 6b mark the outline of the EM field packets at the two connection junctions between the branches and the main wire. It is interesting that the plasmon packet position of zigzag pattern with strong EM near-field intensity overlapped with the position of the junction between the main wire and the C branch wire for the inputs corresponding to Figure 5b. In order to make NOT gate works well, this kind near-field distribution at the branch junction position is crucial to obtain sufficient interference between two plasmon beams (one launched in the main wire, and another one in the branch) to make the output intensity sufficiently small. For plasmonic OR gate, significant interference is not required. Strong interference requires that two beams should meet closely at the beginning, i.e., the node position with strong EM intensity should overlap with the connecting junction. Hence, the degree of such overlapping will determine how well the beams interfere.

If the polarization of I1 input is rotated to be about  $130^\circ$  as shown in Figure 6c, the zigzag EM near-field distribution pattern is dramatically changed from that in Figure 6bi. In Figure 6c, the intense EM field packet of the zigzag pattern is completely moved away from the C branch junction, while the I2 branch junction now overlaps with an intense EM field packet. The interference between C and I1 becomes much less strong as shown in Figure 6d (red curve), while the interference between I1 and I2 becomes much stronger (black curve). The interference depth, i.e. the ratio of maximum and minimum output intensity ( $I_{max}/I_{min}$ ) when the phase of two plasmon beams differs by  $\pi$ , can be tuned by shifting

the zigzag EM wave packet on or off the branch junctions with different incident polarization on the primary wire (Figure 6e).

## 5. SUMMARY

In simple photonic networks composed of Ag NWs, a complete family of Boolean logic gates is demonstrated by interference of plasmon beams launched at different input terminals. Furthermore, a plasmonic NOR gate is demonstrated by cascading OR gate and NOT gate. We use QD as local reporters to image the local electric field distribution of propagating SPs along Ag NWs, which provides a valuable tool for the study of plasmons propagating in NW networks. The underlying physical mechanism for the logic operations is that the plasmon interferences modulate the near field distribution and thus control the output intensity. To realized the cascaded NOR gate, the plasmon packet should overlap with the junction between the main wire and the control branch. These findings shed new light onto both fundamental understanding of propagating plasmons in complex networks and may advance the development of integrated plasmonic devices for new generation information technologies.

## ACKNOWLEDGEMENTS

This work was supported by NSFC Grants (Nos.10625418, 10874233 and 11004237), MOST Grants (Nos. 2006DFB02020 and 2009CB930700), the "Bairen Project", "Knowledge Innovation Project" (KJ CX2-EW-W04) and the "Visiting Professorship for Senior International Scientists" of CAS.

## REFERENCES

- [1] Moskovits, M., "Surface-enhanced Raman spectroscopy: a brief retrospective," *J. Raman Spectrosc.* 36, 485-496 (2005).
- [2] Lakowicz, J. R., Shen, Y. B., D'Auria, S., Malicka, J., Fang, J. Y., Gryczynski, Z. and Gryczynski, I., "Radiative decay engineering 2. Effects of silver island films on fluorescence intensity, lifetimes, and resonance energy transfer," *Anal. Biochem.* 301, 261-277 (2002).
- [3] Kall, M., Xu, H. X. and Johansson, P., "Field enhancement and molecular response in surface-enhanced Raman scattering and fluorescence spectroscopy," *J. Raman Spectrosc.* 36, 510-514 (2005).
- [4] Xu, H. X., Wang, X. H., Persson, M. P., Xu, H. Q., Kall, M. and Johansson, P., "Unified treatment of fluorescence and Raman scattering processes near metal surfaces," *Phys. Rev. Lett.* 93, 243002 (2004).
- [5] Xu, H. X. and Kall, M., "Surface-plasmon-enhanced optical forces in silver nanoaggregates," *Phys. Rev. Lett.* 89, 246802 (2002).
- [6] Svedberg, F., Li, Z. P., Xu, H. X. and Kall, M., "Creating hot nanoparticle pairs for surface-enhanced Raman spectroscopy through optical manipulation," *Nano Lett.* 6, 2639-2641 (2006).
- [7] Li, Z. P., Kall, M. and Xu, H., "Optical forces on interacting plasmonic nanoparticles in a focused Gaussian beam," *Phys. Rev. B* 77, 085412 (2008).
- [8] Xu, H. X. and Kall, M., "Modeling the optical response of nanoparticle-based surface plasmon resonance sensors," *Sens. Actuator B-Chem.* 87, 244-249 (2002).
- [9] Zhou, Y., Xu, H., Dahlin, A. B., Vallkil, J., Borrebaeck, C. A. K., Wingren, C., Liedberg, B. and Hook, F., "Quantitative interpretation of gold nanoparticle-based bioassays designed for detection of immunocomplex formation," *Biointerphases* 2, 6-15 (2007).
- [10] Willets, K. A. and Van Duyne, R. P., "Localized surface plasmon resonance spectroscopy and sensing," *Annu. Rev. Phys. Chem.* 58, 267-297 (2007).
- [11] Lal, S., Clare, S. E. and Halas, N. J., "Nanoshell-Enabled Photothermal Cancer Therapy: Impending Clinical Impact," *Accounts Chem. Res.* 41, 1842-1851 (2008).
- [12] Atwater, H. A. and Polman, A., "Plasmonics for improved photovoltaic devices," *Nature Mater.* 9, 205-213 (2010).

- [13] Xu, H. X., "Electromagnetic energy flow near nanoparticles - I: single spheres," *J. Quant. Spectrosc. Radiat. Transf.* 87, 53-67 (2004).
- [14] Xu, H. X., Bjerneld, E. J., Kall, M. and Borjesson, L., "Spectroscopy of single hemoglobin molecules by surface enhanced Raman scattering," *Phys. Rev. Lett.* 83, 4357-4360 (1999).
- [15] Xu, H. X., Aizpurua, J., Kall, M. and Apell, P., "Electromagnetic contributions to single-molecule sensitivity in surface-enhanced Raman scattering," *Phys. Rev. E* 62, 4318-4324 (2000).
- [16] Xu, H. X., "A new method by extending Mie theory to calculate local field in outside/inside of aggregates of arbitrary spheres," *Phys. Lett. A* 312, 411-419 (2003).
- [17] Xu, H. X., "Calculation of the near field of aggregates of arbitrary spheres," *J. Opt. Soc. Am. A-Opt. Image Sci. Vis.* 21, 804-809 (2004).
- [18] Xu, H. X. and Kall, M., "Estimating SERS properties of silver-particle aggregates through generalized Mie theory," [Surface-Enhanced Raman Scattering: Physics and Applications], Springer, 87-103 (2006).
- [19] Tong, L. M., Li, Z. P., Zhu, T., Xu, H. X. and Liu, Z. F., "Single gold-nanoparticle-enhanced Raman scattering of individual single-walled carbon nanotubes via atomic force microscope manipulation," *J. Phys. Chem. C* 112, 7119-7123 (2008).
- [20] Prikulis, J., Xu, H., Gunnarsson, L., Kall, M. and Olin, H., "Phase-sensitive near-field imaging of metal nanoparticles," *J. Appl. Phys.* 92, 6211-6214 (2002).
- [21] Xu, H. X. and Kall, M., "Polarization-dependent surface-enhanced Raman spectroscopy of isolated silver nanoaggregates," *Chemphyschem* 4, 1001-1005 (2003).
- [22] Xu, H. X., "Theoretical study of coated spherical metallic nanoparticles for single-molecule surface-enhanced spectroscopy," *Appl. Phys. Lett.* 85, 5980-5982 (2004).
- [23] Xu, H. X., "Multilayered metal core-shell nanostructures for inducing a large and tunable local optical field," *Phys. Rev. B* 72, 073405 (2005).
- [24] Zhao, K., Xu, H. X., Gu, B. H. and Zhang, Z. Y., "One-dimensional arrays of nanoshell dimers for single molecule spectroscopy via surface-enhanced Raman scattering," *J. Chem. Phys.* 125, 081102 (2006).
- [25] Wang, W., Li, Z. P., Gu, B. H., Zhang, Z. Y. and Xu, H. X., "Ag@SiO<sub>2</sub> Core-Shell Nanoparticles for Probing Spatial Distribution of Electromagnetic Field Enhancement via Surface-Enhanced Raman Scattering," *ACS Nano* 3, 3493-3496 (2009).
- [26] Gunnarsson, L., Petronis, S., Kasemo, B., Xu, H., Bjerneld, E. J. and Kall, M., "Optimizing nanofabricated substrates for surface enhanced Raman scattering," *Nanostruct. Mater.* 12, 783 (1999).
- [27] Gunnarsson, L., Bjerneld, E. J., Xu, H., Petronis, S., Kasemo, B. and Kall, M., "Interparticle coupling effects in nanofabricated substrates for surface-enhanced Raman scattering," *Appl. Phys. Lett.* 78, 802-804 (2001).
- [28] Wei, H., Hakanson, U., Yang, Z. L., Hook, F. and Xu, H. X., "Individual nanometer hole-particle pairs for surface-enhanced Raman scattering," *Small* 4, 1296-1300 (2008).
- [29] Wei, H., Hao, F., Huang, Y. Z., Wang, W. Z., Nordlander, P. and Xu, H. X., "Polarization dependence of surface-enhanced Raman scattering in gold nanoparticle-nanowire systems," *Nano Lett.* 8, 2497-2502 (2008).
- [30] Chen, J. N., Yang, W. S., Dick, K., Deppert, K., Xu, H. Q., Samuelson, L. and Xu, H. X., "Tip-enhanced Raman scattering of p-thiocresol molecules on individual gold nanoparticles," *Appl. Phys. Lett.* 92, 093110 (2008).
- [31] Yang, Z. L., Aizpurua, J. and Xu, H. X., "Electromagnetic field enhancement in TERS configurations," *J. Raman Spectrosc.* 40, 1343-1348 (2009).
- [32] Wei, H. and Xu, H., "Surface-enhanced Raman scattering of lambda-DNA," *Appl. Phys. A-Mater. Sci. Process.* 89, 273-275 (2007).
- [33] Li, Z. P. and Xu, H. X., "Electromagnetic energy flow near metal nanoparticles - II: Algorithms for the calculation of the light scattering of multi-spheres and photon energy transport via linear chains of Ag nanoparticles," *J. Quant. Spectrosc. Radiat. Transf.* 103, 394-401 (2007).
- [34] Chen, J. N., Martensson, T., Dick, K. A., Deppert, K., Xu, H. Q., Samuelson, L. and Xu, H. X., "Surface-enhanced Raman scattering of rhodamine 6G on nanowire arrays decorated with gold nanoparticles," *Nanotechnology* 19, 275712 (2008).
- [35] Liang, H. Y., Li, Z. P., Wang, W. Z., Wu, Y. S. and Xu, H. X., "Highly Surface-roughened Flower-like Silver Nanoparticles for Extremely Sensitive Substrates of Surface-enhanced Raman Scattering," *Adv. Mater.* 21, 4614-4618 (2009).
- [36] Zhang, B., Xu, P., Xie, X. M., Wei, H., Li, Z. P., Mack, N. H., Han, X. J., Xu, H. X. and Wang, H. L., "Acid-directed synthesis of SERS-active hierarchical assemblies of silver nanostructures," *J. Mater. Chem.* 21, 2495-2501 (2011).

- [37] Shegai, T., Li, Z. P., Dadosh, T., Zhang, Z. Y., Xu, H. X. and Haran, G., "Managing light polarization via plasmon-molecule interactions within an asymmetric metal nanoparticle trimer," *Proc. Natl. Acad. Sci. USA* 105, 16448-16453 (2008).
- [38] Li, Z. P., Shegai, T., Haran, G. and Xu, H. X., "Multiple-Particle Nanoantennas for Enormous Enhancement and Polarization Control of Light Emission," *Acs Nano* 3, 637-642 (2009).
- [39] Liang, H. Y., Yang, H. X., Wang, W. Z., Li, J. Q. and Xu, H. X., "High-Yield Uniform Synthesis and Microstructure-Determination of Rice-Shaped Silver Nanocrystals," *J. Am. Chem. Soc.* 131, 6068-6069 (2009).
- [40] Liang, H. Y., Wang, W. Z., Huang, Y. Z., Zhang, S. P., Wei, H. and Xu, H. X., "Controlled Synthesis of Uniform Silver Nanospheres," *J. Phys. Chem. C* 114, 7427-7431 (2010).
- [41] Wei, H., Reyes-Coronado, A., Nordlander, P., Aizpurua, J. and Xu, H. X., "Multipolar Plasmon Resonances in Individual Ag Nanorice," *Acs Nano* 4, 2649-2654 (2010).
- [42] Huang, Y. Z., Wang, W. Z., Liang, H. Y. and Xu, H. X., "Surfactant-Promoted Reductive Synthesis of Shape-Controlled Gold Nanostructures," *Cryst. Growth Des.* 9, 858-862 (2009).
- [43] Ditzbacher, H., Hohenau, A., Wagner, D., Kreibitz, U., Rogers, M., Hofer, F., Aussenegg, F. R. and Krenn, J. R., "Silver nanowires as surface plasmon resonators," *Phys. Rev. Lett.* 95, 257403 (2005).
- [44] Sanders, A. W., Routenberg, D. A., Wiley, B. J., Xia, Y. N., Dufresne, E. R. and Reed, M. A., "Observation of plasmon propagation, redirection, and fan-out in silver nanowires," *Nano Lett.* 6, 1822-1826 (2006).
- [45] Knight, M. W., Grady, N. K., Bardhan, R., Hao, F., Nordlander, P. and Halas, N. J., "Nanoparticle-mediated coupling of light into a nanowire," *Nano Lett.* 7, 2346-2350 (2007).
- [46] Akimov, A. V., Mukherjee, A., Yu, C. L., Chang, D. E., Zibrov, A. S., Hemmer, P. R., Park, H. and Lukin, M. D., "Generation of single optical plasmons in metallic nanowires coupled to quantum dots," *Nature* 450, 402-406 (2007).
- [47] Kolesov, R., Grotz, B., Balasubramanian, G., Stohr, R. J., Nicolet, A. A. L., Hemmer, P. R., Jelezko, F. and Wrachtrup, J., "Wave-particle duality of single surface plasmon polaritons," *Nat. Phys.* 5, 470-474 (2009).
- [48] Fang, Y. R., Wei, H., Hao, F., Nordlander, P. and Xu, H. X., "Remote-Excitation Surface-Enhanced Raman Scattering Using Propagating Ag Nanowire Plasmons," *Nano Lett.* 9, 2049-2053 (2009).
- [49] Wei, H., Ratchford, D., Li, X. Q., Xu, H. X. and Shih, C. K., "Propagating Surface Plasmon Induced Photon Emission from Quantum Dots," *Nano Lett.* 9, 4168-4171 (2009).
- [50] Li, Z. P., Hao, F., Huang, Y. Z., Fang, Y. R., Nordlander, P. and Xu, H. X., "Directional Light Emission from Propagating Surface Plasmons of Silver Nanowires," *Nano Lett.* 9, 4383-4386 (2009).
- [51] Shegai, T., Miljkovic, V. D., Bao, K., Xu, H. X., Nordlander, P., Johansson, P. and Kall, M., "Unidirectional Broadband Light Emission from Supported Plasmonic Nanowires," *Nano Lett.* 11, 706-711 (2011).
- [52] Li, Z. P., Bao, K., Fang, Y. R., Huang, Y. Z., Nordlander, P. and Xu, H. X., "Correlation between Incident and Emission Polarization in Nanowire Surface Plasmon Waveguides," *Nano Lett.* 10, 1831-1835 (2010).
- [53] Li, Z. P., Zhang, S. P., Halas, N. J., Nordlander, P. and Xu, H. X., "Coherent Modulation of Propagating Plasmons in Silver-Nanowire-Based Structures," *Small* 7, 593-596 (2011).
- [54] Li, Z. P., Bao, K., Fang, Y. R., Guan, Z. Q., Halas, N. J., Nordlander, P. and Xu, H. X., "Effect of a proximal substrate on plasmon propagation in silver nanowires," *Phys. Rev. B* 82, 241402 (2010).
- [55] Shegai, T., Huang, Y. Z., Xu, H. X. and Kall, M., "Coloring fluorescence emission with silver nanowires," *Appl. Phys. Lett.* 96, 103114 (2010).
- [56] Fang, Y. R., Li, Z. P., Huang, Y. Z., Zhang, S. P., Nordlander, P., Halas, N. J. and Xu, H. X., "Branched Silver Nanowires as Controllable Plasmon Routers," *Nano Lett.* 10, 1950-1954 (2010).
- [57] Wei, H., Li, Z. P., Tian, X. R., Wang, Z. X., Cong, F. Z., Liu, N., Zhang, S. P., Nordlander, P., Halas, N. J. and Xu, H. X., "Quantum Dot-Based Local Field Imaging Reveals Plasmon-Based Interferometric Logic in Silver Nanowire Networks," *Nano Lett.* 11, 471-475 (2011).
- [58] Wei, H., Wang, Z. X., Tian, X. R., Kall, M. and Xu, H. X., "Cascaded logic gates in nanophotonic plasmon networks," *Nat. Commun.* 2, 387 (2011).